Visualizing grain boundaries in monolayer MoSe$_2$ using mild H$_2$O vapor etching

Jinhuan Wang[1,§], Xiaozhi Xu[2,§], Ruixi Qiao[2,§], Jing Liang[2], Can Liu[2], Bohao Zheng[2], Lei Liu[3], Peng Gao[4], Qingze Jiao[1], Dapeng Yu[5], Yun Zhao[1] (✉), and Kaihui Liu[2,6] (✉)

[1] *School of Chemistry and Chemical Engineering, Beijing Institute of Technology, Beijing 100081, China*

[2] *State Key Laboratory for Mesoscopic Physics, School of Physics, Peking University, Beijing 100871, China*

[3] *Department of Materials Science and Engineering, College of Engineering, Peking University, Beijing 100871, China*

[4] *International Centre for Quantum Materials, and Electron Microscopy Laboratory, School of Physics, Peking University, Beijing 100871, China*

[5] *Department of Physics, South University of Science and Technology of China, Shenzhen 518055, China*

[6] *Collaborative Innovation Centre of Quantum Matter, Beijing 100871, China*

[§] *Jinhuan Wang, Xiaozhi Xu and Ruixi Qiao contributed equally to this work.*

ABSTRACT

Beyond graphene, two-dimensional (2D) transition metal dichalcogenides (TMDs) have attracted significant attention owing to their potential in next-generation nanoelectronics and optoelectronics. Nevertheless, grain boundaries are ubiquitous in large-area as-grown TMD materials and would significantly affect their band structure, electrical transport, and optical properties. Therefore, the characterization of grain boundaries is essential for engineering the properties and optimizing the growth in TMD materials. Although the existence of boundaries can be measured using scanning tunneling microscopy, transmission electron microscopy, or nonlinear optical microscopy, a universal, convenient, and accurate method to detect boundaries with a twist angle over a large scale is still lacking. Herein, we report a high-throughput method using mild hot H$_2$O etching to visualize grain boundaries of TMDs under an optical microscope, while ensuring that the method is nearly noninvasive to grain domains. This technique utilizes the reactivity difference between stable grain domains and defective grain boundaries and the mild etching capacity of hot water vapor. As grain boundaries of two domains with twist angles have defective lines, this method enables to visualize all types of grain boundaries unambiguously. Moreover, the characterization is based on an optical microscope and therefore naturally of a large scale. We further demonstrate the successful application of this method to other TMD materials such as MoS$_2$ and WSe$_2$. Our technique facilitates the large-area characterization of grain boundaries and will accelerate the controllable growth of large single-crystal TMDs.

Address correspondence to Kaihui Liu, khliu@pku.edu.cn; Yun Zhao, zhaoyun@bit.edu.cn

1 Introduction

Atomically layered two-dimensional (2D) materials, ranging from graphene and molybdenum disulfide to black phosphorus and others have gained widespread research interest owing to their fascinating properties and numerous applications. 2D transition metal dichalcogenides (TMDs), such as MX_2 (M = Mo, W; X = S, Se, Te), are the most prominent 2D materials after graphene. A thickness-dependent band structure [1, 2], circular dichroism [3–6], high on/off current ratio [7, 8], valley-spin locking effect [9–11], and strong light–matter interactions [11–14] of TMDs have been discovered. Significant potential in future electronics [15–17], optoelectronics [18–22], valleytronics [23, 24], and catalysts [25–29] have also been demonstrated. It is widely believed that TMDs will be a very important building block in future nanotechnology [30–32].

Despite these exciting merits, the inherent properties of TMDs can be easily influenced by grain boundaries [33–37]. Sometimes, these defects can introduce many novel properties such as band gap variation [33], longitudinal acoustic mode [34], edge nonlinear optics [35, 36], and significantly improved catalytic activity [25]. However, usually, the grain boundaries are defective and degrade the electrical/thermal transport and optoelectronic properties [37]. In the ideal materials design, a large-sized single crystal without grain boundaries is always a long-term pursuit. To eliminate the grain boundaries in TMDs, an effective and accurate technique to visualize grain boundaries over a large scale is a prerequisite. Until now, numerous efforts have been made to investigate the grain boundaries of TMDs [38–47] and other 2D materials [48–52]. Transmission electron microscopy (TEM) and scanning tunneling microscopy can provide accurate information of the boundary structure with atomic-level spatial resolution, but both fail to characterize large-scale materials [41]. Optical nonlinear second-harmonic generation (SHG) [35, 36] or third-harmonic generation (THG) have also been applied to observe the grain boundaries [45]; exposure of nematic liquid crystal thin layer on TMD surface to visualize the grain boundaries under an optical

polarized microscope has also been developed [46]. However, the above optical techniques become invalid when the twist angle of the two domains is close to zero [35, 36]. Raman or photoluminescence (PL) spectroscopy also enables to characterize the grain boundaries, but the mechanism is still under debate. UV irradiation or high-temperature oxidation may be used to visualize boundaries over a large scale [41, 42]. Nevertheless, these treatments may damage the grain domain and induce ambiguity in the identification of grain boundaries [41, 42]. An effective and accurate technique to visualize grain boundaries with an inter-domain twist angle over a large scale is still lacking.
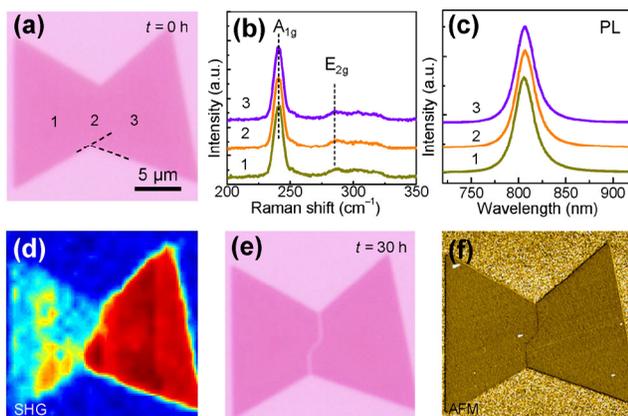
Herein, we report a high-throughput method for visualizing grain boundaries of TMDs over a large scale using an optical microscope. After exposure to hot water vapor, the grain boundaries of TMDs are mildly oxidized with evident optical contrast, whereas the grain domains themselves maintain their intact lattice structure. This technique is based on the reactivity difference between grain domains and defective grain boundaries and the mild etching capacity of hot water vapor. As grain boundaries of two domains with a twist angle are defective lines, this method enables to visualize all types of grain boundaries unambiguously. We also successfully apply this method to characterize other TMD materials such as MoS_2 and WSe_2, where only the treatment time required is different. Our results provide a convenient and accurate approach to visualize grain boundaries and would accelerate the controllable growth of large single crystals of TMD materials.

2 Results and discussions

In our experiment, monolayer $MoSe_2$, MoS_2, and WSe_2 were synthesized on 300-nm-thick SiO_2/Si via chemical vapor deposition (CVD) (see Experimental for details of the growth process). Owing to D_{3h} lattice symmetry, the domains are triangular in shape (Fig. S1 in the Electronic Supplementary Material (ESM)), and thus, we can easily obtain their crystalline orientation information [39, 40]. To study the grain boundary information of $MoSe_2$, two merged

domains with twist angle ~ 50° (θ, defined using the corresponding relative edge directions) were chosen and investigated in detail (Fig. 1(a)). Raman and PL spectra obtained at the two $MoSe_2$ domains and the merged area show no distinct difference (Figs. 1(b) and 1(c)), and thus, it is difficult to directly detect the boundary. Further, as the boundary is only atomic wide, it cannot be observed even using scanning electron microscopy (SEM) or atomic force microscopy (AFM) in our experiment (Fig. S2 in the ESM). Recently, the SHG technique has been used to probe grain boundaries in MoS_2 because it is strongly dependent on the lattice orientation and light polarization [35, 36]. Using this method, we visualized the grain boundary of the two merged domains (Fig. 1(d)). However, this technique requires time-consuming SHG mapping, and becomes invalid when the twist angle is close to zero [35, 36].
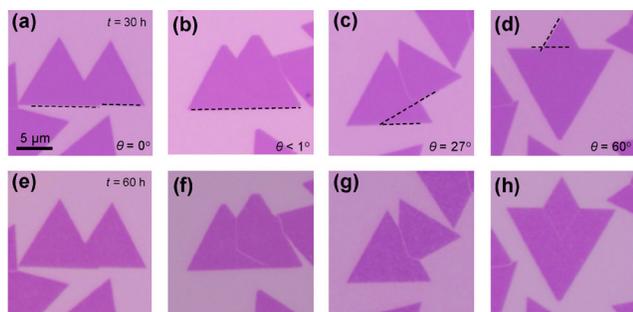
As water vapor is a well-known mild reactant and has been used to etch amorphous carbon on carbon

nanotubes or graphene [53, 54], it is sufficiently active to etch the defective grain boundaries and sufficiently inert not to attack grain domains in $MoSe_2$. To test our design, an as-grown $MoSe_2$ sample was exposed to hot water vapor at 50 °C. After mild treatment for 30 h, the grain boundary shown in Fig. 1(d) was observed using an optical microscope, but the $MoSe_2$ grain domains did not show any observable changes (Fig. 1(e)). AFM and SEM measurements were thereafter conducted to observe the morphology of the grain boundary and domains. As expected, the domain boundary could be observed under both AFM and SEM after hot vapor treatment (Fig. 1(f) and Figs. S3 and S4 in the ESM) and the surface roughness of the grain domains was almost the same as that of the as-grown $MoSe_2$ (Fig. S5 in the ESM). The domain surface was very clean and the dirty spots reported with previous wild etching methods could be avoided [41, 42]. We further applied our technique to a large-area continuous $MoSe_2$ film and observed that the boundaries were evident (Fig. S6 in the ESM), demonstrating the capability of our technique for probing grain boundaries in large-scale $MoSe_2$ films.

We further conducted control experiments to qualitatively determine the capability of visualizing grain boundaries formed between two domains with different twist angles. Four typical configurations were chosen with the twist angles of 0°, < 1°, 27°, and 60°. After hot vapor treatment for 30 h, the grain boundaries for the sample with twist angles of 0°, < 1°, and 60° did not appear but the sample with θ = 27° exhibited grain boundaries (Figs. 2(a)–2(d)). Upon further treatment with hot vapor for 60 h, boundary lines appeared on domains with θ = 60° and < 1° as well (Figs. 2(f) and 2(h)) and the boundary line of the domains with θ = 27° became evident (Fig. 2(g)). We also observed that very small domains (such as the one on the right side of Fig. 2(b)) disappeared after etching (Fig. 2(f)). This is because the H_2O vapor etching occurs at both boundaries and edges and the very small domains can be etched away over a long time. However, no boundary lines could be observed for the two domains with θ = 0° (Fig. 2(e)), even after treatment for more than 300 h

Figure 1 Probing grain boundaries of $MoSe_2$ with optical microscopy. (a) Optical image of two merged $MoSe_2$ domains with a twist angle of ~ 50° on 300-nm-thick SiO_2/Si substrate. (b) Raman spectra of $MoSe_2$ at regions 1, 2, and 3 marked in (a). Peaks at 244 and 287 cm^{-1} correspond to A_{1g} and E_{2g} modes, respectively. (c) PL spectra of $MoSe_2$ at regions 1, 2, and 3 marked in (a). The identical peaks show that it is difficult to detect the boundary using Raman or PL measurements. (d) SHG mapping of $MoSe_2$ sample shown in (a). A clear boundary line appears owing to the distinctive polarization-dependent SHG intensities of the two domains. (e) Optical image of the merged $MoSe_2$ domains after hot vapor etching for 30 h at 50 °C. The boundary line is the same as that shown in (d). (f) AFM phase image of the merged $MoSe_2$ domains after hot vapor etching. The boundary line is consistent with that in (d) and (e). The image sizes of (a) and (d)–(f) are the same.

Figure 2 Etched grain boundaries between domains with different twist angles. (a)–(d) Optical images of two MoSe$_2$ domains with the twist angles θ = 0°, < 1°, 27°, and 60° after hot water vapor etching for 30 h. (e) and (f) Optical images after etching for 60 h. Only the two domains with zero twist angle (merged into a big domain without grain boundary) show no etching line, and grain boundary lines are unambiguously visualized between domains with a non-zero twist angle. The image sizes of (a)–(h) are the same.

(Fig. S7 in the ESM). Previous results show that only two domains with θ = 0° can merge into a large domain and do not have a grain boundary (the so-called epitaxial growth with seamless stitching) [50–52]. It is also observed that the grain boundary with θ = 60° is more stable than that of the others, which originates from the special twin boundary structure with θ = 60° [55]. As a defective grain boundary line is ubiquitous between the domains of any non-zero twist angles, our technique is applicable to any kind of grain boundaries. This is a significant advantage over the previous SHG/THG mapping or liquid-crystal-assisted polarization method, where only domain boundaries with non-zero twist angle (typically θ > 2°) are visible.

To further confirm that the optically visible line between the two merged domains is the grain boundary rather than the cracks or other additional changes introduced during the treatment, aberration-corrected TEM (AC-TEM) was used to characterize the atomic structure and the lattice orientations near and at the visualized boundary line. After the exposure to hot vapor, MoSe$_2$ samples were transferred onto TEM grids (See Experimental for transfer details). High-angle annular dark-field scanning transmission electron microscopic (HAADF-STEM) image shown in Fig. 3(a) is a typical area with three merged domains, where etched grain boundary lines can be observed at the merged region. Subsequently, atomically
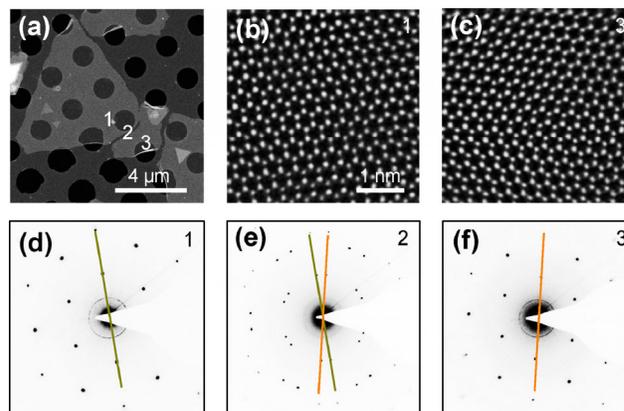
Figure 3 Atomic-level characterizations of grain boundary after etching. (a) Low-magnification STEM image of MoSe$_2$ domains with clear boundary lines transferred onto TEM grid. (b) and (c) Atomically resolved HAADF-STEM images of MoSe$_2$ at region 1 (b) and region 3 (c) marked in (a). The atomic structure of the two MoSe$_2$ domains are twisted by 13°. The overall defect-free atomic images shown in (b) and (c) confirm the noninvasiveness of the mild etching method. (d)–(f) The SAED patterns of MoSe$_2$ at regions 1 (d), 2 (e), and 3 (f) marked in (a). The SAED patterns are consistent with the atomic structure (b) and (c), and a twist angle of 13° is identified (e).

resolved STEM characterizations were conducted on the two domains near the grain boundary line (Figs. 3(b) and 3(c)). The atomic lattices of MoSe$_2$ on the two sides of the domain boundary line are twisted with an angle of 13°, demonstrating that domains separated by the boundary line have different lattice orientations. Furthermore, selected-area electron diffraction (SAED) measurements were carried out to further confirm the lattice orientations. The SAED patterns of the two domains (Figs. 3(d) and 3(f)) and the merged area (Fig. 3(e)) are consistent with the atomic lattice structure, and a twist angle of 13° is again observed (Fig. 3(e)). In other words, the TEM characterizations confirm that the visible lines appearing after the hot vapor treatment are the grain boundaries.

The atomic images in the grain domain area also reveal negligible defects after treatment (Figs. 3(b) and 3(c)), which confirms that the mild H$_2$O vapor etching is nearly noninvasive to the grain domains, as expected. The noninvasive characteristic can also be evaluated using Raman and PL spectra (Fig. 4). The three characteristic peaks corresponding to A$_{1g}$ and E$_{2g}$ modes retain their both position and amplitude after the treatment [56]. The PL peak redshifts by ~ 4 meV
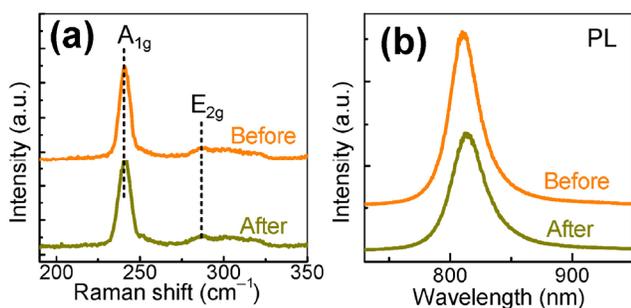
Figure 4 Noninvasive characteristics of the mild etching on grain domains of MoSe$_2$. (a) Representative Raman spectra of MoSe$_2$ obtained before and after the hot water vapor treatment. The intensity and position of the peaks corresponding to A$_{1g}$ and E$_{2g}$ modes change negligibly. (b) Representative PL spectra of MoSe$_2$ obtained before and after the hot vapor treatment. The intensity and position of the peaks changes only slightly. Both (a) and (b) indicate the noninvasive characteristics of our mild etching technique.

and the integrated intensity decreases by only ~ 20% (induced by the charging effect from water adsorption) [57]. These results are in striking contrast to other wild etching techniques where the amplitude in both Raman and PL spectra decreases significantly [41, 42], which proves that mild water vapor is noninvasive to MoSe$_2$ grain domains.

To assess the versatility of our technique, WSe$_2$ and MoS$_2$ were thereafter tested using the same strategy. Grain boundaries in both WSe$_2$ and MoS$_2$ appeared after the hot vapor treatment (Figs. 5(a) and 5(b)). Notably, the required treatment time can be different for different TMD materials (Fig. 5(c)), indicating the material-dependent boundary stability. The MoS$_2$ grain boundary is the most stable one, which is evident considering that MoS$_2$ is widely used as a
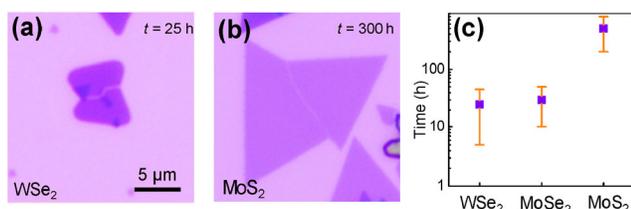
Figure 5 Versatility of the mild etching technique for other TMD materials. (a) and (b) Optical images of WSe$_2$ and MoS$_2$ domains after the hot vapor treatment. The domain boundaries can be visualized using an optical microscope. (c) The required treatment time for different TMD materials. The time difference reflects the boundary stability between them. The error bars originate from the different inter-domain twist angles.

lubricant (as a solid lubricant, it must be sufficiently stable to avoid easy degradation in air).

3 Conclusions

In conclusion, we report an effective grain boundary visualization method for TMDs over a large scale using an optical microscope via mild hot water vapor etching. The boundaries of TMDs were etched and could be observed optically with clear contrast. This method can probe grain boundaries of any twist angle but is noninvasive to grain domains. This convenient method can visualize grain boundaries effectively and accurately, which can help to verify whether the TMDs samples are single crystals and in turn to help optimize the growth procedure and therefore, it should accelerate the controllable growth of large single-crystals of TMDs.

4 Experimental

4.1 Growth of MoSe$_2$ domains

We grew MoSe$_2$ on SiO$_2$/Si substrate using the CVD method with MoO$_3$ and Se powder as precursors. Accordingly, 20.0 mg of MoO$_3$ powder was placed at the center of a tube furnace and 40.0 mg of Se powder was placed at the upstream side 13 cm from the MoO$_3$ powder. Substrates were placed on the crucible containing MoO$_3$ powder. The CVD process was performed under ambient pressure and controlled ultrahigh-purity Argon gas. The method of preparation is as follows: maintained at 105 °C, gas flow of 500 sccm for 1 h, ramped to 800 °C with gas flow of 15 sccm for 50 min, maintained at 800 °C with gas flow of 15 sccm for 10 min, and thereafter naturally cooled down to room temperature.

4.2 MoSe$_2$ transfer onto TEM grids

The MoSe$_2$ sample for TEM characterization was prepared using a standard polymethyl methacrylate (PMMA)-assisted transfer method. The MoSe$_2$ sample was spin-coated with PMMA and baked at 150 °C for 5 min. Thereafter, 1 M NaOH solution was used to etch the SiO$_2$ substrate and PMMA/MoSe$_2$ film floats on the surface of the solution. The PMMA/MoSe$_2$ film

was thereafter washed with deionized water for five times. Finally, the PMMA/MoSe$_2$ film was scooped out with a TEM grid (GIG-1010-4C, Beijing Zhongjingkeyi Technology Co., Ltd.) and dried under ambient conditions for 6 h. PMMA was removed with acetone subsequently.

4.3   Material characterization

Raman spectra were obtained using a homemade Raman system with the laser excitation wavelength of 532 nm and power of ~ 1 mW. Optical images were obtained using an Olympus BX51 microscope. SHG mapping was obtained using the same system combined with a piezo stage and controller (Physik Instrumente P-333.3CD and E-725). Samples were excited using a femtosecond OPO laser centered at 820 nm with the average power of 800 μW (Spectra-Physics Inspire ultrafast OPO system with pulse duration of 100 fs and repetition rate of 80 MHz). The excitation photon was normally incident and linearly polarized. At each point, the parallel component of the generated SHG signal was selected by a linear polarizer before applying the grating spectrograph (Princeton SP-2500i). AFM measurements were performed using Bruker Dimensional ICON under atmospheric environment. STEM experiments were performed in an FEI Titan Themis G2 300 operated at 300 kV with low electron dose to minimize the beam damage.

Electronic Supplementary Material: Supplementary material (extra optical, SEM, and AFM images of boundaries of TMDs) is available in the online version of the article at https://doi.org/10.1007/s12274-018-1991-2.

References

[1]   Mak, K. F.; Lee, C.; Hone, J.; Shan, J.; Heinz, T. F. Atomically thin MoS$_2$: A new direct-gap semiconductor. *Phys. Rev. Lett.* **2010**, *105*, 136805.

[2]   Splendiani, A.; Sun, L.; Zhang, Y. B.; Li, T. S.; Kim, J.; Chim, C. Y.; Galli, G.; Wang, F. Emerging photoluminescence in monolayer MoS$_2$. *Nano Lett.* **2010**, *10*, 1271–1275.

[3]   Cao, T.; Wang, G.; Han, W. P.; Ye, H. Q.; Zhu, C. R.; Shi, J. R.; Niu, Q.; Tan, P. H.; Wang, E.; Liu, B. L. et al. Valley-selective circular dichroism of monolayer molybdenum disulphide. *Nat. Commun.* **2012**, *3*, 887.

[4]   Mak, K. F.; He, K. L.; Shan, J.; Heinz, T. F. Control of valley polarization in monolayer MoS$_2$ by optical helicity. *Nat. Nanotechnol.* **2012**, *7*, 494–498.

[5]   Zeng, H. L.; Dai, J. F.; Yao, W.; Xiao, D.; Cui, X. D. Valley polarization in MoS$_2$ monolayers by optical pumping. *Nat. Nanotechnol.* **2012**, *7*, 490–493.

[6]   Jones, A. M.; Yu, H. Y.; Ghimire, N. J.; Wu, S. F.; Aivazian, G.; Ross, J. S.; Zhao, B.; Yan, J. Q.; Mandrus, D. G.; Xiao, D. et al. Optical generation of excitonic valley coherence in monolayer WSe$_2$. *Nat. Nanotechnol.* **2013**, *8*, 634–638.

[7]   Radisavljevic, B.; Radenovic, A.; Brivio, J.; Giacometti, V.; Kis, A. Single-layer MoS$_2$ transistors. *Nat. Nanotechnol.* **2011**, *6*, 147–150.

[8]   Kang, K.; Xie, S. E.; Huang, L. J.; Han, Y. M.; Huang, P. Y.; Mak, K. F.; Kim, C. J.; Muller, D.; Park, J. High-mobility three-atom-thick semiconducting films with wafer-scale homogeneity. *Nature* **2015**, *520*, 656–660.

[9]   Xiao, D.; Liu, G. B.; Feng, W. X.; Xu, X. D.; Yao, W. Coupled spin and valley physics in monolayers of MoS$_2$ and other group-VI dichalcogenides. *Phys. Rev. Lett.* **2012**, *108*, 196802.

[10] Mak, K. F.; McGill, K. L.; Park, J.; McEuen, P. L. The valley hall effect in MoS$_2$ transistors. *Science* **2014**, *344*, 1489–1492.

[11] Kim, J.; Hong, X. P.; Jin, C. H.; Shi, S. F.; Chang, C. Y. S.; Chiu, M. H.; Li, L. J.; Wang, F. Ultrafast generation of pseudo-magnetic field for valley excitons in WSe$_2$ monolayers. *Science* **2014**, *346*, 1205–1208.

[12] Qiu, D. Y.; da Jornada, F. H.; Louie, S. G. Optical spectrum of MoS$_2$: Many-body effects and diversity of exciton states. *Phys. Rev. Lett.* **2013**, *111*, 216805.

[13] Ye, Z. L.; Cao, T.; O'Brien, K.; Zhu, H. Y.; Yin, X. B.; Wang, Y.; Louie, S. G.; Zhang, X. Probing excitonic dark states in single-layer tungsten disulphide. *Nature* **2014**, *513*, 214–218.

[14] Wang, G.; Marie, X.; Gerber, I.; Amand, T.; Lagarde, D.; Bouet, L.; Vidal, M.; Balocchi, A.; Urbaszek, B. Giant

enhancement of the optical second-harmonic emission of WSe$_2$ monolayers by laser excitation at exciton resonances. *Phys. Rev. Lett.* **2015**, *114*, 097403.

[15] Koppens, F. H. L.; Mueller, T.; Avouris, P.; Ferrari, A. C.; Vitiello, M. S.; Polini, M. Photodetectors based on graphene, other two-dimensional materials and hybrid systems. *Nat. Nanotechnol.* **2014**, *9*, 780–793.

[16] Zhang, H. Ultrathin two-dimensional nanomaterials. *ACS Nano* **2015**, *9*, 9451–9469.

[17] Chhowalla, M.; Jena, D.; Zhang, H. Two-dimensional semiconductors for transistors. *Nat. Rev. Mater.* **2016**, *1*, 16052.

[18] Wang, Q. H.; Kalantar-Zadeh, K.; Kis, A.; Coleman, J. N.; Strano, M. S. Electronics and optoelectronics of two-dimensional transition metal dichalcogenides. *Nat. Nanotechnol.* **2012**, *7*, 699–712.

[19] Yin, Z. Y.; Li, H.; Li, H.; Jiang, L.; Shi, Y. M.; Sun, Y. H.; Lu, G.; Zhang, Q.; Chen, X. D.; Zhang, H. Single-layer MoS$_2$ phototransistors. *ACS Nano* **2012**, *6*, 74–80.

[20] Xia, F. N.; Wang, H.; Xiao, D.; Dubey, M.; Ramasubramaniam, A. Two-dimensional material nanophotonics. *Nat. Photonics* **2014**, *8*, 899–907.

[21] Mak, K. F.; Shan, J. Photonics and optoelectronics of 2D semiconductor transition metal dichalcogenides. *Nat. Photonics* **2016**, *10*, 216–226.

[22] Zhang, W. J.; Wang, Q. X.; Chen, Y.; Wang, Z.; Wee, A. T. S. Van der waals stacked 2D layered materials for optoelectronics. *2D Mater* **2016**, *3*, 022001.

[23] Xu, X. D.; Yao, W.; Xiao, D.; Heinz, T. F. Spin and pseudospins in layered transition metal dichalcogenides. *Nat. Phys.* **2014**, *10*, 343–350.

[24] Schaibley, J. R.; Yu, H. Y.; Clark, G.; Rivera, P.; Ross, J. S.; Seyler, K. L.; Yao, W.; Xu, X. D. Valleytronics in 2D materials. *Nat. Rev. Mater.* **2016**, *1*, 16055.

[25] Jaramillo, T. F.; Jørgensen, K. P.; Bonde, J.; Nielsen, J. H.; Horch, S.; Chorkendorff, I. Identification of active edge sites for electrochemical H$_2$ evolution from MoS$_2$ nanocatalysts. *Science* **2007**, *317*, 100–102.

[26] Chhowalla, M.; Shin, H. S.; Eda, G.; Li, L. J.; Loh, K. P.; Zhang, H. The chemistry of two-dimensional layered transition metal dichalcogenide nanosheets. *Nat. Chem.* **2013**, *5*, 263–275.

[27] Lu, Q. P.; Yu, Y. F.; Ma, Q. L.; Chen, B.; Zhang, H. 2D transition-metal-dichalcogenide-nanosheet-based composites for photocatalytic and electrocatalytic hydrogen evolution reactions. *Adv. Mater.* **2016**, *28*, 1917–1933.

[28] Zhang, X.; Lai, Z. C.; Tan, C. L.; Zhang, H. Solution-processed two-dimensional MoS$_2$ nanosheets: Preparation, hybridization, and applications. *Angew. Chem., Int. Ed.* **2016**, *55*, 8816–8838.

[29] Tan, C. L.; Cao, X. H.; Wu, X. J.; He, Q. Y.; Yang, J.; Zhang, X.; Chen, J. Z.; Zhao, W.; Han, S. K.; Nam, G. H. et al. Recent advances in ultrathin two-dimensional nanomaterials. *Chem. Rev.* **2017**, *117*, 6225–6331.

[30] Britnell, L.; Ribeiro, R. M.; Eckmann, A.; Jalil, R.; Belle, B. D.; Mishchenko, A.; Kim, Y. J.; Gorbachev, R. V.; Georgiou, T.; Morozov, S. V. et al. Strong light-matter interactions in heterostructures of atomically thin films. *Science* **2013**, *340*, 1311–1314.

[31] Geim, A. K.; Grigorieva, I. V. Van der waals heterostructures. *Nature* **2013**, *499*, 419–425.

[32] Novoselov, K. S.; Mishchenko, A.; Carvalho, A.; Neto, A. H. C. 2D materials and van der waals heterostructures. *Science* **2016**, *353*, aac9439.

[33] Huang, Y. L.; Chen, Y. F.; Zhang, W. J.; Quek, S. Y.; Chen, C. H.; Li, L. J.; Hsu, W. T.; Chang, W. H.; Zheng, Y. J.; Chen, W. et al. Bandgap tunability at single-layer molybdenum disulphide grain boundaries. *Nat. Commun.* **2015**, *6*, 6298.

[34] Xu, H.; Liu, S. L.; Ding, Z. J.; Tan, S. J. R.; Yam, K. M.; Bao, Y.; Nai, C. T.; Ng, M. F.; Lu, J.; Zhang, C. et al. Oscillating edge states in one-dimensional MoS$_2$ nanowires. *Nat. Commun.* **2016**, *7*, 12904.

[35] Yin, X. B.; Ye, Z. L.; Chenet, D. A.; Ye, Y.; O'Brien, K.; Hone, J. C.; Zhang, X. Edge nonlinear optics on a MoS$_2$ atomic monolayer. *Science* **2014**, *344*, 488–490.

[36] Cheng, J. X.; Jiang, T.; Ji, Q. Q.; Zhang, Y.; Li, Z. M.; Shan, Y. W.; Zhang, Y. F.; Gong, X. G.; Liu, W. T.; Wu, S. W. Kinetic nature of grain boundary formation in as-grown MoS$_2$ monolayers. *Adv. Mater.* **2015**, *27*, 4069–4074.

[37] Yu, Z. H.; Pan, Y. M.; Shen, Y. T.; Wang, Z. L.; Ong, Z. Y.; Xu, T.; Xin, R.; Pan, L. J.; Wang, B. G.; Sun, L. T. et al. Towards intrinsic charge transport in monolayer molybdenum disulfide by defect and interface engineering. *Nat. Commun.* **2014**, *5*, 5290.

[38] Zhang, Y.; Zhang, Y. F.; Ji, Q. Q.; Ju, J.; Yuan, H. T.; Shi, J. P.; Gao, T.; Ma, D. L.; Liu, M. X.; Chen, Y. B. et al. Controlled growth of high-quality monolayer WS$_2$ layers on sapphire and imaging its grain boundary. *ACS Nano* **2013**, *7*, 8963–8971.

[39] Najmaei, S.; Liu, Z.; Zhou, W.; Zou, X. L.; Shi, G.; Lei, S. D.; Yakobson, B. I.; Idrobo, J. C.; Ajayan, P. M.; Lou, J. Vapour phase growth and grain boundary structure of molybdenum disulfide atomic layers. *Nat. Mater.* **2013**, *12*, 754–759.

[40] van der Zande, A. M.; Huang, P. Y.; Chenet, D. A.; Berkelbach, T. C.; You, Y. M.; Lee, G. H.; Heinz, T. F.; Reichman, D. R.; Muller, D. A.; Hone, J. C. Grains and grain boundaries in highly crystalline monolayer molybdenum disulphide. *Nat. Mater.* **2013**, *12*, 554–561.

[41] Ly, T. H.; Chiu, M. H.; Li, M. Y.; Zhao, J.; Perello, D. J.;

Cichocka, M. O.; Oh, H. M.; Chae, S. H.; Jeong, H. Y.; Yao, F. et al. Observing grain boundaries in CVD-grown monolayer transition metal dichalcogenides. *ACS Nano* **2014**, *8*, 11401–11408.

[42] Rong, Y. M.; He, K.; Pacios, M.; Robertson, A. W.; Bhaskaran, H.; Warner, J. H. Controlled preferential oxidation of grain boundaries in monolayer tungsten disulfide for direct optical imaging. *ACS Nano* **2015**, *9*, 3695–3703.

[43] Azizi, A.; Zou, X. L.; Ercius, P.; Zhang, Z. H.; Elias, A. L.; Perea-López, N.; Stone, G.; Terrones, M.; Yakobson, B. I.; Alem, N. Dislocation motion and grain boundary migration in two-dimensional tungsten disulphide. *Nat. Commun.* **2014**, *5*, 4867.

[44] Park, S.; Kim, M. S.; Kim, H.; Lee, J.; Han, G. H.; Jung, J.; Kim, J. Spectroscopic visualization of grain boundaries of monolayer molybdenum disulfide by stacking bilayers. *ACS Nano* **2015**, *9*, 11042–11048.

[45] Karvonen, L.; Säynätjoki, A.; Huttunen, M. J.; Autere, A.; Amirsolaimani, B.; Li, S. S.; Norwood, R. A.; Peyghambarian, N.; Lipsanen, H.; Eda, G. et al. Rapid visualization of grain boundaries in monolayer MoS₂ by multiphoton microscopy. *Nat. Commun.* **2017**, *8*, 15714.

[46] Shehzad, M. A.; Hussain, S.; Lee, J.; Jung, J.; Lee, N.; Kim, G.; Seo, Y. Study of grains and boundaries of molybdenum diselenide and tungsten diselenide using liquid crystal. *Nano Lett.* **2017**, *17*, 1474–1481.

[47] Ly, T. H.; Zhao, J.; Cichocka, M. O.; Li, L. J.; Lee, Y. H. Dynamical observations on the crack tip zone and stress corrosion of two-dimensional MoS₂. *Nat. Commun.* **2017**, *8*, 14116.

[48] Duong, D. L.; Han, G. H.; Lee, S. M.; Gunes, F.; Kim, E. S.; Kim, S. T.; Kim, H.; Ta, Q. H.; So, K. P.; Yoon, S. J. et al. Probing graphene grain boundaries with optical microscopy. *Nature* **2012**, *490*, 235–239.

[49] Kim, D. W.; Kim, Y. H.; Jeong, H. S.; Jung, H. T. Direct visualization of large-area graphene domains and boundaries by optical birefringency. *Nat. Nanotechnol.* **2012**, *7*, 29–34.

[50] Lee, J. H.; Lee, E. K.; Joo, W. J.; Jang, Y.; Kim, B. S.; Lim, J. Y.; Choi, S. H.; Ahn, S. J.; Ahn, J. R.; Park, M. H. et al. Wafer-scale growth of single-crystal monolayer graphene on reusable hydrogen-terminated germanium. *Science* **2014**, *344*, 286–289.

[51] Nguyen, V. L.; Shin, B. G.; Duong, D. L.; Kim, S. T.; Perello, D.; Lim, Y. J.; Yuan, Q. H.; Ding, F.; Jeong, H. Y.; Shin, H. S. et al. Seamless stitching of graphene domains on polished copper (111) foil. *Adv. Mater.* **2015**, *27*, 1376–1382.

[52] Xu, X. Z.; Zhang, Z. H.; Dong, J. C.; Yi, D.; Niu, J. J.; Wu, M. H.; Lin, L.; Yin, R. K.; Li, M. Q.; Zhou, J. Y. et al. Ultrafast epitaxial growth of metre-sized single-crystal graphene on industrial Cu foil. *Sci. Bull.* **2017**, *62*, 1074–1080.

[53] Hata, K.; Futaba, D. N.; Mizuno, K.; Namai, T.; Yumura, M.; Iijima, S. Water-assisted highly efficient synthesis of impurity-free single-walled carbon nanotubes. *Science* **2004**, *306*, 1362–1364.

[54] Zhang, R. F.; Zhang, Y. Y.; Zhang, Q.; Xie, H. H.; Qian, W. Z.; Wei, F. Growth of half-meter long carbon nanotubes based on Schulz–Flory distribution. *ACS Nano* **2013**, *7*, 6156–6161.

[55] Barja, S.; Wickenburg, S.; Liu, Z. F.; Zhang, Y.; Ryu, H. J.; Ugeda, M. M.; Hussain, Z.; Shen, Z. X.; Mo, S. K.; Wong, E. et al. Charge density wave order in 1D mirror twin boundaries of single-layer MoSe₂. *Nat. Phys.* **2016**, *12*, 751–756.

[56] Chang, Y. H.; Zhang, W. J.; Zhu, Y. H.; Han, Y.; Pu, J.; Chang, J. K.; Hsu, W. T.; Huang, J. K.; Hsu, C. L.; Chiu, M. H. et al. Monolayer MoSe₂ grown by chemical vapor deposition for fast photodetection. *ACS Nano* **2014**, *8*, 8582–8590.

[57] Ni, Z. H.; Wang, H. M.; Luo, Z. Q.; Wang, Y. Y.; Yu, T.; Wu, Y. H.; Shen, Z. X. The effect of vacuum annealing on graphene. *J. Raman Spectrosc.* **2010**, *41*, 479–483.